ARL-TR-8191 ● Oct 2017

US Army Research Laboratory

A Comparison of Hybrid Reynolds-averaged Navier-Stokes/Large-Eddy Simulation (RANS/LES) and Unsteady RANS Predictions of Separated Flow for a Variable-Speed Power-Turbine Blade Operating with Low Inlet Turbulence Levels

by David T Booth

NOTICES

Disclaimers

The findings in this report are not to be construed as an official Department of the Army position unless so designated by other authorized documents.

Citation of manufacturer's or trade names does not constitute an official endorsement or approval of the use thereof.

Destroy this report when it is no longer needed. Do not return it to the originator.

ARL-TR-8191 ● OCT 2017

US Army Research Laboratory

A Comparison of Hybrid Reynolds-averaged Navier-Stokes/Large-Eddy Simulation (RANS/LES) and Unsteady RANS Predictions of Separated Flow for a Variable-Speed Power-Turbine Blade Operating with Low Inlet Turbulence Levels

by David T Booth
Vehicle & Technology Directorate, ARL

REPORT DOCUMENTATION PAGE

Form Approved
OMB No. 0704-0188

1. REPORT DATE *(DD-MM-YYYY)*	2. REPORT TYPE	3. DATES COVERED (From - To)
October 2017	Technical Report	10/1/2016 – 09/30/17

4. TITLE AND SUBTITLE

A Comparison of Hybrid Reynolds-averaged Navier-Stokes/Large-Eddy Simulation (RANS/LES) and Unsteady RANS Predictions of Separated Flow for a Variable-Speed Power-Turbine Blade Operating with Low Inlet Turbulence Levels

5a. CONTRACT NUMBER

5b. GRANT NUMBER

5c. PROGRAM ELEMENT NUMBER

6. AUTHOR(S)

David T Booth

5d. PROJECT NUMBER

5e. TASK NUMBER

5f. WORK UNIT NUMBER

7. PERFORMING ORGANIZATION NAME(S) AND ADDRESS(ES)

US Army Research Laboratory
ATTN: RDRL-VTD
Aberdeen Proving Ground, MD 21005-5066

8. PERFORMING ORGANIZATION REPORT NUMBER

ARL-TR-8191

9. SPONSORING/MONITORING AGENCY NAME(S) AND ADDRESS(ES)

10. SPONSOR/MONITOR'S ACRONYM(S)

11. SPONSOR/MONITOR'S REPORT NUMBER(S)

12. DISTRIBUTION/AVAILABILITY STATEMENT

Approved for public release; distribution is unlimited.

13. SUPPLEMENTARY NOTES

14. ABSTRACT

A comparison of hybrid Reynolds-averaged Navier-Stokes/Large-Eddy Simulation (RANS/LES) and unsteady RANS computations for unsteady separated flow prediction of a linear turbine blade cascade operating with large incidence angle variation is described. The computations comprise a periodic single blade that represents the midspan section of a variable-speed power-turbine blade that was tested in NASA Glenn Research Center's Transonic Turbine Blade Cascade Facility. A commercial, off-the-shelf software package, Pointwise and CFD++, was used for the grid generation and computations. Simulations were assessed at low inlet turbulence levels for positive and negative incidence angles that represent turbine cruise and takeoff conditions. Comparisons of results for blade loading and loss were made to test data from the transonic tunnel. Comparisons of results for separation predictions were made between the hybrid RANS/LES and RANS computations. Comparisons of separation prediction revealed significant differences in location and extent of separation between the models and grid types.

15. SUBJECT TERMS

power-turbine, CFD, hybrid RANS/LES, Reynolds-averaged Navier-Stokes, large-eddy simulation, turbine blade cascade

16. SECURITY CLASSIFICATION OF:			17. LIMITATION OF ABSTRACT	18. NUMBER OF PAGES	19a. NAME OF RESPONSIBLE PERSON
a. REPORT	b. ABSTRACT	c. THIS PAGE			David T Booth
Unclassified	Unclassified	Unclassified	UU	39	19b. TELEPHONE NUMBER (Include area code) 410-278-9206

Contents

List of Figures

List of Tables

Acknowledgments

DT Booth thanks AB Flegel and PW Giel for providing the experimental information and data used in this paper.

1. Introduction

This study is part of an effort underway at the US Army Research Laboratory (ARL) to develop modeling and simulation capabilities of turbine blade aerodynamics. Transition, separation, and complex flow physics occur with the variable-speed power-turbine (VSPT) due to operation at low Reynolds numbers and a wide range of incidence angles. Improving prediction of separation at low and high turbulence intensities, Reynolds numbers, and Mach numbers is an important area of research as flow separation has a large impact on turbine blade efficiency and performance. The hybrid Reynolds-averaged Navier-Stokes/Large Eddy Simulation (RANS/LES) approach is considered a promising technique to use in high Reynolds number separated flow cases and has been used in a wide range of applications.[1] The hybrid RANS/LES approach was chosen over LES to avoid the higher computational cost and to take advantage of the accuracy of RANS prediction of attached boundary layers and the stronger prediction capability of LES in the separated flow regions.[2] The higher fidelity of the hybrid RANS/LES technique as compared to RANS may be needed to resolve the flow features necessary for accurate prediction of separation and to better assist in the design of power-turbines such as the VSPT. Evaluation and comparison of the hybrid RANS/LES and unsteady RANS capabilities of a commercial off-the-shelf (COTS) software was performed using a 3-D model of a candidate VSPT blade midspan section of a notional large civil tilt-rotor vehicle.

Power-turbine blades of conventional rotorcraft turboshaft engines are optimized to operate at nearly a fixed speed and a fixed incidence angle. The VSPT is a potential enabling technology for high-speed tilt-rotor aircraft where the power-turbine speed is slowed down by as much as 51% during cruise flight compared to takeoff (hover) flight.[3] Significant design challenges exist for the VSPT due to this speed change, such as high work factors at cruise, large incidence angle variation (40° to 60°), and low aft stage Reynolds numbers at 28 kft cruise flight.[4] Incidence tolerant turbine blade research was conducted by NASA Glenn Research Center (GRC) and ARL as a potential solution for maintaining turbine blade aerodynamic performance for variable-speed power-turbines.

Experiments were performed on a candidate VSPT blade midspan section in the Transonic Turbine Blade Cascade Facility at NASA GRC.[5,6] The experimental data of Flegel-McVetta et al.[5] and Flegel et al.[6] were acquired at low and high inlet turbulence intensities, over a range of Reynolds numbers, at engine/mission-relevant exit Mach numbers, and over a wide range of incidence angles: +15.8° to –51.0°. The inlet flow of the experiment was well characterized in terms of inlet

boundary-layer thickness, inlet turbulence intensity, and dissipation/length-scale using 2-point hotwire measurements. Because the Reynolds numbers of the tunnel were higher than in the VSPT application, Flegel-McVetta et al.[5] chose to test without an inlet turbulence grid so that the flow would be transitional, mimicking low Reynolds operation at engine-relevant turbulence intensities. The experimental results indicate the design/cruise condition of the VSPT blade is highly loaded with transitional flow, while the takeoff condition represents an extreme off-design operating condition where the blade row is unloaded and the flow is very 2-D across the blade surface.[7]

Several simplifications exist with the turbine blade cascade facility compared to a power-turbine in a gas turbine engine. The cascade facility has geometry simplifications of being a linear, nonrotating set of turbine blades where the blade cross-section is constant in the spanwise direction and does not include a tip gap at the end. Differences in the operating environment include non-heated inlet air and absence of combustion gases. Simplifications that cause differences in the nature of the flow include the lack of a wake from stator blades and lack of rotational effects associated with Coriolis and centrifugal acceleration fields, the relative motion of the endwall, and impact of unsteadiness of downstream blade rows on the flow.[8] Therefore, the nature of transition mechanism in the turbine blade cascade is flow instability and separation-induced transition as opposed to bypass transition, which is the main transition mechanism in a gas turbine engine that occurs due to wakes from stators.[9] Nonetheless, the facility allows for highly 3-D flow and is useful for studying the aerodynamic effects of large incidence angle and Reynolds number changes, which are key challenges for VSPT applications.

Computational Fluid Dynamics (CFD) computations were performed at the turbine cruise condition corresponding to an inflow angle of 40° and a takeoff condition of the blade corresponding to an inflow angle of –2.5°. These conditions were operating at low inlet turbulence intensity that will admit transitional flow on the blade surface, which is a significant challenge of the VSPT application.[4] Both conditions were at the lowest Reynolds number tested, which was at 40% of the design point Reynolds number condition. This low Reynolds number was chosen to reduce the computational cost of the simulations. The computations were compared to measured blade loading and midspan loss provided by Flegel-McVetta et al.[5] Comparisons of separation prediction of hybrid RANS/LES computations were made to time accurate RANS computations of the VSPT cascade blade.

2. Experimental Description

The following is a summary of the experimental test that was conducted in the Transonic Turbine Blade Cascade Facility located at NASA GRC. Details of the experiment are given in Flegel-McVetta et al.[5,6]

2.1 Facility

The Transonic Turbine Blade Cascade Facility is a large-scale cascade that allows detailed flow field surveys and blade surface measurements.[10–12] The facility has a continuous run capability over a large relevant range of Reynolds and Mach numbers along with the ability to vary incidence over a 95° range. Details of the facility are shown in Fig. 1.

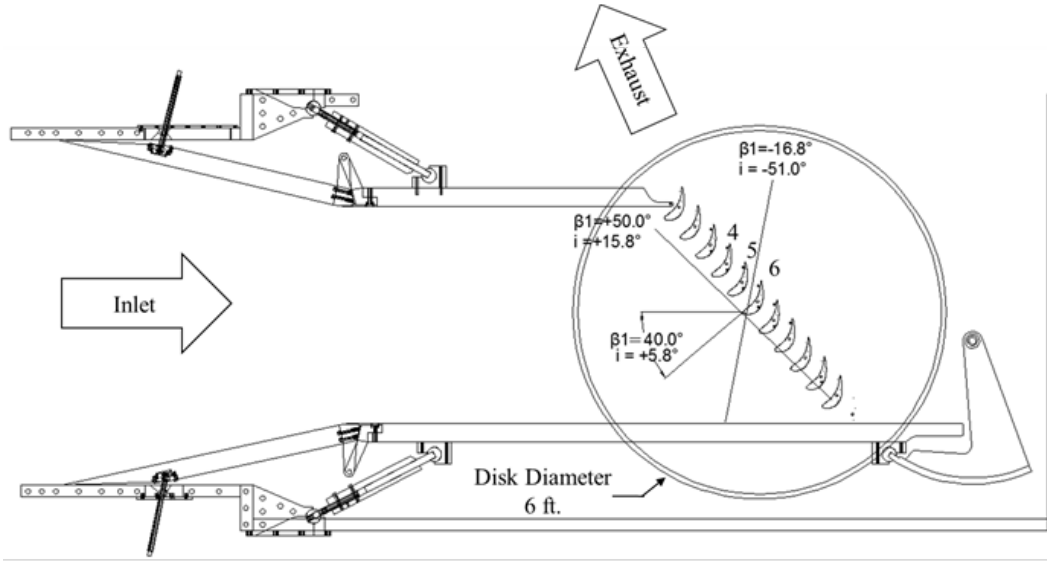

Fig. 1 Transonic turbine blade cascade facility

The cascade was made up of nominally 11 blades. The blade geometry is a scaled midspan section of a VSPT second stage rotor.[13] Details of the blade geometry are shown in Fig. 2 and described in Table 1. Data were acquired for 10 incidence angles spanning $+15.8° \leq i \leq -51.0°$.[5,6] Two design incidence angles that correspond to takeoff ($i = -36.7°$) and cruise ($i = +5.8°$) were the focus of this CFD study. The design pressure ratio, *PR*, was 1.412, which corresponds to an exit isentropic Mach number of 0.72. A baseline flow condition was established by finding the lowest Reynolds number at which the tunnel could consistently

maintain an exit Mach number of 0.72. The baseline Reynolds number, Re_b, was found to be 0.53×10^6.[14] The experimental data used for this CFD study were taken at test conditions at 40% Re_b and 77% PR (Table 2).

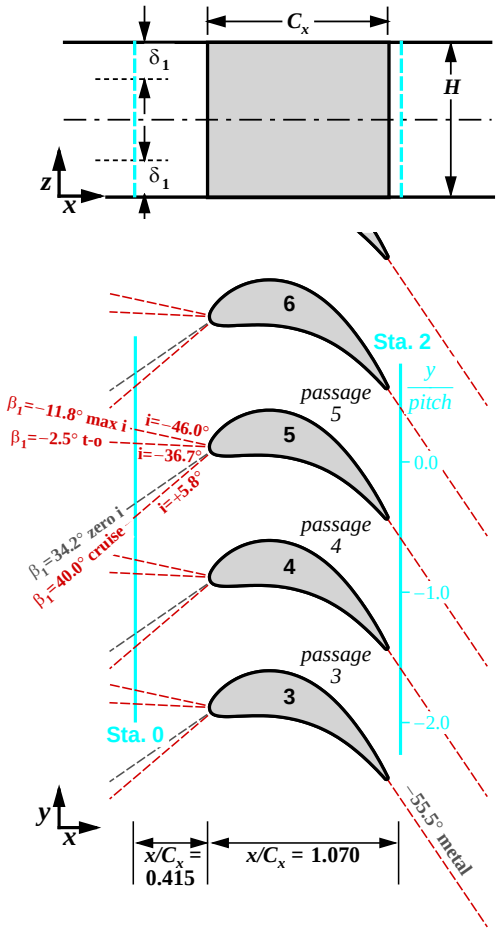

Fig. 2 VSPT blade details and measurement station locations

Table 1 VSPT blade description

Geometry	Value
Axial Chord, C_x	180.57 mm (7.109 inches)
True Chord	194.44 mm (7.655 inches)
Pitch, S	130.00 mm (5.119 inches)
Span, H	152.40 mm (6.000 inches)
Throat diameter	72.85 mm (2.868 inches)
Leading edge diameter	15.16 mm (0.597 inches)
Trailing edge diameter	3.30 mm (0.130 inches)
Stagger angle	20.35°
Inlet metal angle	34.2°
Uncovered turning	19.47°
Exit metal angle	−55.54°

Table 2 Angle and flow conditions used in the simulations

Incidence Angle, i	Inlet Angle, β_1	Inlet Re_{Cx}	Exit Re_{Cx}	PR	Exit M_{is}	δ_{inlet} in.
−36.7° (Takeoff)	−2.5°	128,600	215,900	1.0886	0.350	1.69
+5.8° (Cruise)	+40.0°	170,300	221,500	1.0891	0.351	1.63

2.2 Measurement Description

Total pressure data were acquired using a 5-hole and 3-hole pneumatic pressure probe installed 0.7 C_x downstream of the blade trailing edge.[14] This survey location is shown as Station 2 in Fig. 2 and traverses across 3 blade passages. For the i = −36.7° and i = +5.8° incidence angles, detailed half-span surveys were acquired over 26 spanwise and 62 pitchwise points. The overall estimated uncertainty in flow angle was ±1.5° and the overall estimated uncertainty in total pressure coefficient was ±0.8%.[5]

The primary measurement blades 4, 5, and 6 were instrumented with pressure static taps located along 10%, 15%, 30%, and 50% span. Blade 5 was fully instrumented with 44 static taps on the pressure and suction side. To verify periodicity, blade 4 had redundant taps located on the suction side of the blade where blade 6 had taps located on the pressure side. The blade static pressures were measured by an electronically scanned pressure system with ±15 psid modules referenced to atmosphere. A 5-point calibration was performed automatically at least once per

hour against a high accuracy quartz pressure transducer. The absolute uncertainty of the pressure measurements was believed to be well within ±0.01 psi.[14]

The inlet turbulence intensity, *Tu*, was characterized with a single-wire hotwire anemometer that was installed in the Station 0 survey plane.[11] A low *Tu* of 0.325% was measured for the test conditions used in this study.[5]

3. Computational Approach

This section contains the description of the computational approach used in the study. The first subsection highlights salient features of the flow solver, the second subsection describes the CFD mesh and mesh generation process, and the third subsection presents the computational parameters of the simulations.

3.1 Flow Solver

The 3-D time-resolved hybrid RANS/LES and RANS computations were performed on structured grids at 2 flow conditions, cruise and takeoff, of the VSPT blade. Computations were run in parallel on a Department of Defense Supercomputing Resource Center supercomputer. A COTS code was used with multi-block grids. For this study, CFD++ version 16.1.1 was the chosen COTS software.[15]

The selected equation set is a pressure-based compressible perfect gas Navier-Stokes solver. The spatial discretization used by the code is a multidimensional total variation diminishing polynomial interpolation determined through limited reconstructions over cells and/or nodes.[16] Spatial discretization is second order with node-based polynomials. The local Courant number is used to accelerate convergence and a second order dual time-stepping technique is selected for time accurate computations.

A Batten-Goldberg hybrid RANS/LES model was used for the hybrid RANS/LES simulations. This model uses a modified form of the classical Smagorinsky model away from the walls and uses a 2-equation nonlinear (cubic) k-epsilon turbulence model on RANS-type grids.[16] The cubic k-epsilon model solves for the turbulence kinetic energy (k) and its dissipation rate (epsilon) and contains nonlinear terms that account for normal-stress anisotropy, swirl, and streamline curvature effects.[15] For the LES simulations, a subgrid scale (SGS) model in the code was implemented that removes the underlying numerical diffusion from the Smagorinsky eddy viscosity SGS model, which results in the model behaving less diffusive in free shear layers.[17] In attached boundary layers RANS is the method used by the model. The model is resistant to ambiguous grid densities and permits the activation of

RANS and LES in different flow regions providing a balanced numerical approach to complex turbulent flows.[1,18,19]

RANS computations were performed for comparison to the hybrid RANS/LES results. Two turbulence models were used for the RANS comparisons, including the 2-equation realizable k-epsilon model and the 4-equation Langtry-Menter transition prediction model. The k-epsilon model uses the Boussinesq relation to obtain Reynolds-stresses algebraically from the modeled eddy viscosity and the available mean-strain tensor.[16] The Langtry-Menter transition prediction model is a 4-equation turbulence closure that solves transport equations for k, turbulence inverse time-scale (ω), intermittency, and transition momentum thickness Reynolds number.[16] An algebraic transition prediction model was used in conjunction with the realizable k-epsilon turbulence model that is based on modifying the generation term, applied to both k- and epsilon transport equations.[16] These turbulence and transition models were chosen for the RANS simulations as previous RANS model comparison work showed that they had better agreement with the design condition experimental data for the VSPT cascade blade than other models tested that were present in the CFD++ code.[14] In addition, prior comparisons of these models were performed by Metacomp Technologies, Inc. using an Aerospatiale A airfoil and S809 airfoil example. The k-epsilon and Algebraic I models and the Langtry-Menter model had the best agreement with the data for these examples.[14] Further evaluations of these models are presented in this paper using the VSPT cascade experimental flow conditions described in Section 2.

3.2 CFD Mesh

A 3-D structured multiblock hybrid RANS/LES mesh was generated from the experimental blade coordinate data using Pointwise version 17.3[20] and is depicted in Fig. 3. The computational domain of the grid includes a single blade with periodic boundary conditions in the pitchwise directions as a representation of a periodic linear cascade. This representation was chosen to simplify the model and reduce the amount of computational resources needed for the simulation and it was assumed that accuracy would be similar in comparison to a full cascade passage model. Only the middle section of the blade that is outside the experimentally measured boundary layer of the endwalls was modelled. This section represents 20% of the actual span. A symmetry boundary condition was used for the spanwise direction. The inlet boundary condition was located at approximately 0.415 C_x upstream of the blade leading edge to correspond to the location of experimental inlet measurement station 0. The exit boundary condition was located approximately 1.0 C_x downstream of the trailing edge to correctly capture the wake region. A back pressure imposition boundary condition was placed there to match

the measured exit pressure. The grid was rotated about the center of the blade in the z-direction to change the incidence of the blade with respect to the incoming flow, which is fixed in the x-direction.

RANS computations were performed in the attached boundary layer region of the turbine blade where higher aspect ratio cells are used. A boundary layer grid thickness of 0.0084 m was used based on the maximum thickness at the blade trailing edge, which was estimated using a one-seventh power law equation for turbulent flow on a flat plate.[21] In the boundary layer region, the grid was constructed so that an initial distance from the wall to the first wall-adjacent centroid, Δy_{init}, of 1.3×10^{-6} m was chosen for a y+ value less than 0.5. A 1.1 expansion factor was used until reaching the region outside the boundary layer where uniform grid cells were used for the LES computations. A total of 54 points were used in the boundary layer normal to the blade surface.

Cells in the LES region of the grid were constructed to be as isotropic as possible, approximating (dx = dy = dz). Cell length in the LES region was determined based on the recommended formulation of $\delta/10$, where δ represents the boundary layer thickness on the blade.[1] Based on an estimated maximum laminar boundary layer thickness value for δ of 2.7×10^{-3} m, cell length was chosen to be 2.7×10^{-4} m.

Dimensions of the grid were 996 × 224 × 130 nodes in the streamwise, pitchwise, and spanwise directions, respectively. There were 1,172 cells around the airfoil with the entire grid containing 32 million cells. Determination of grid fineness was based on recommendations for similar grids used for LES computations for low pressure turbine blades summarized in a survey performed by Ameri in 2016.[22]

A coarser 3-D structured mesh was used for hybrid RANS/LES grid sensitivity study and RANS computation comparisons. For this grid the boundaries were similar to the hybrid RANS/LES mesh except the mesh includes the endwall and models half the span due to symmetry in the spanwise direction. There was no blade tip gap and a viscous no-slip wall boundary condition was used for the endwall boundary. A Musker inlet velocity profile boundary condition was used for the inlet boundary. This boundary condition provided by the CFD++ code for internal flow parallel to one or more solid walls allows the user to prescribe a fully-developed turbulent boundary-layer profile for all mean-flow and turbulence-related quantities. The generated boundary-layer profile is based on Musker's 1979 formulation[16] in conjunction with a compressibility transformation and temperature fit due to Van Driest.[16] Turbulence quantities in the boundary layer are determined as functions of the mean-velocity derivatives, based on an assumption of local equilibrium.

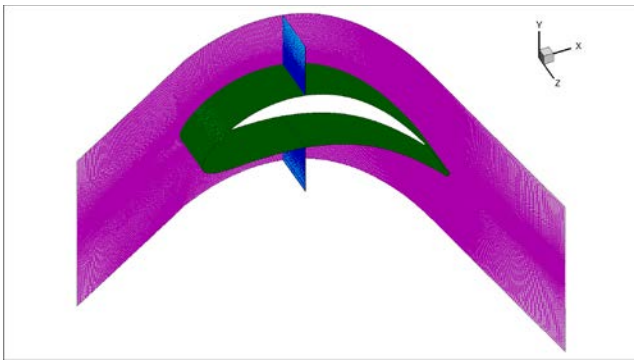

Fig. 3 3-D grid of VSPT blade

A boundary layer grid with a thickness of 2.0 inches was used to accurately resolve the viscous boundary layer of the endwall that was determined using an estimated maximum thickness based on the experimental data. A Δy_{init} of 2.0×10^{-4} inches was chosen with a tanh boundary layer spacing and a 1.1 expansion factor to obtain 73 points in the boundary layer normal to the wall. A boundary layer grid was created for the blade in the same way with a Δy_{init} of 3.0×10^{-5} inches and 69 points in the boundary layer normal to the blade surface.

Dimensions of the grid were 480 × 167 × 78 nodes in streamwise, pitchwise and spanwise directions, respectively. There were 784 cells around the airfoil with the entire grid containing 8-million cells. Previous grid sensitivity analysis of this grid was performed using RANS computations that showed solution results were independent of grid refinement at 4 million cells so it was expected that the 8-million cell grid would perform adequately for the RANS computations presented in this paper.[14]

3.3 Computational Parameters

Computations were performed at the cruise and takeoff conditions listed of +40° and -2.5°, respectively. A low *Tu* level of 0.325% was used to match experimental estimations.[5] A turbulence length scale of 0.026 m was used for the computations. This value was based on length scale measurements made for the NASA Energy Efficient Engine turbine blade tested at similar *Tu* and M in the GRC Transonic Turbine Blade Cascade Facility.[23]

Due to the unsteady nature of the flow through the VSPT cascade at the takeoff condition at low inlet turbulence levels, as determined by Booth et al. 2015,[14] time accurate computations were performed. For temporal resolution, a time step of 2×10^{-6} s based on the ratio of mesh spacing in the unsteady wake region to maximum relevant wave speed was used. Implicit dual time stepping with 10 subiterations was used. Time of flight through the blade passage was estimated

to be 0.002 s. This resulted in 1000 time steps for one flow-through. After convergence of the solution was obtained, the solutions were time averaged over approximately 20 flow-through times to have sufficient data for statistical analysis.

For solution convergence, computations were carried out until sufficient reduction was obtained for the transient residuals from the inner (subiteration) steps of the dual time-stepping simulations. The residuals are the full right-hand side (RHS) for the quasi steady-state inner problem, such as shown in the equation below

$$\frac{\partial(\vec{q}V)}{\partial t} + \frac{\partial(\vec{q}V)}{\partial \tau} + \vec{F}_{inv} + \vec{F}_{visc} + \vec{S} \cdot V = 0 \tag{1}$$

or

$$\frac{\partial(\vec{q}V)}{\partial \tau} = -\underbrace{\left(\frac{\partial(\vec{q}V)}{\partial t} + \vec{F}_{inv} + \vec{F}_{visc} + \vec{S} \cdot V\right)}_{RHS}, \tag{2}$$

where $\vec{q}$ is the dependent variable vector, $V$is the cell volume, τ is the pseudo time, $\vec{F}_{inv}$ is the inviscid flux, $\vec{F}_{visc}$ is the viscous flux, and $\vec{S}$ is the source term.[16] At each pseudo time step, for each equation in each cell, the absolute value of the RHS is computed and the residuals are the average of this quantity over all cells for each equation.[16] The solutions were considered to have converged when the inner residuals had reduced by at least 0.05.

4. Results and Discussion

The main objective of the study is to investigate the computational accuracy of the hybrid RANS/LES method in predicting the unsteady separated flow of the VSPT blade. The results were compared to time accurate RANS computations and experimental data for the cruise and takeoff angles. Comparisons of computational results were made to experimental measurements for blade loading and the wake region. Comparison of flow separation predictions were made between hybrid RANS/LES and RANS methods using velocity streamline plots.

4.1 Cruise Angle

4.1.1 Pressure Distribution

Comparisons of hybrid RANS/LES and time accurate RANS computational results to the experimental measurements of the blade pressure distributions were made. Figure 4 compares solutions to experiment for blade surface pressures for the cruise condition at the 50% span location. Figure 4a compares results using the 32-million-cell grid and Fig. 4b compares results using the 8-million cell grid.

Experimental results were measured on 3 consecutive blades in the cascade, blades 4 through 6, as shown in the legend.

As shown in Fig. 4a, good agreement is observed between hybrid RANS/LES computations and experimental data (black circles) with exception to the region on the suction side from approximately 60% chord to the trailing edge where results become poor. The hybrid RANS/LES computations appear to predict a suction side separation/reattachment at $x/C_x = 0.85 – 0.95$ that does not match the experimental data, which suggests a separation/reattachment at $x/C_x = 0.6 – 0.8$. As shown in Fig. 4b, plots of results for the hybrid RANS/LES model using the coarser grid show overall good agreement, and then agreement becomes very poor after 60% chord on the suction side and after 90% chord on the pressure side. A separation appears to be predicted at 95% chord that is also not consistent with the location suggested by the experimental data. Overall results for the hybrid RANS/LES computations are poorer for the 8-million cell grid, which is possibly due to it being too coarse for LES computations.

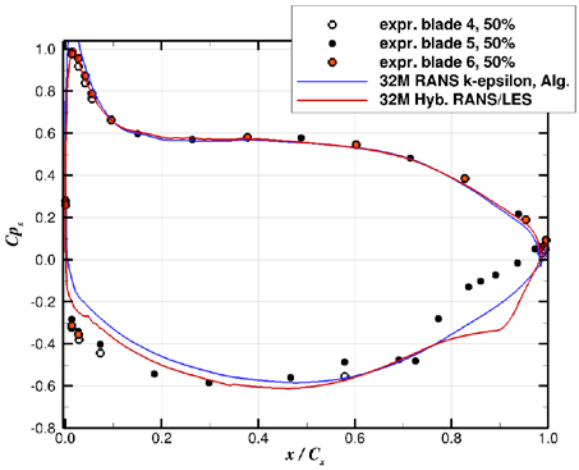

(a)

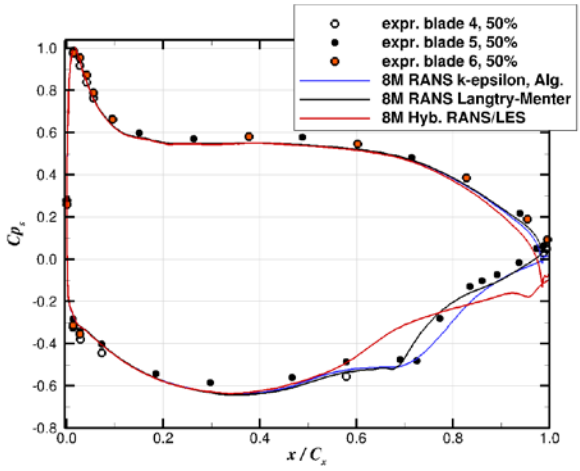

(b)

Fig. 4 Comparison of hybrid RANS/LES and RANS computations to experiment for cruise condition pressure distributions at 50% span; a) 32M grid and b) 8M grid

Overall, for the RANS computations, very good agreement is observed for both models using the 8-million cell grid as shown in Fig. 4b. At x/C_x = 0.6 – 0.8, the computations accurately predict the suction side separation/reattachment at midspan suggested by the experimental data. Pressure side agreement with the data is also excellent. RANS computations using the 32-million-cell grid were good until approximately 60% chord on the suction side, where the computations fail to predict the separation/reattachment suggested by experiment. The difference in results between the 2 grids for RANS computations suggests that there are significant endwall effects in the flow that affect the suction side after the 50% chord location and the 8-million-cell grid, which models the endwall, is able to accurately capture these effects.

4.1.2 Exit Total Pressure

Comparisons of computational results to experimental measurements for the blade wake region were made. Figure 5 compares plots of computed and measured midspan total pressure loss at 7% C_x downstream of the blade. Results with the 32-million cell grid matched the location of the wake better than the 8-million cell grid for both hybrid RANS/LES and RANS models; however, they both predicted a narrower wake and underpredicted the maximum Cp_t value. In addition, RANS computed values of Cp_t outside the wake become negative in value below the pressure side of the blade, which is inconsistent with the data. All results with the 8-million-cell grid overpredicted the size and magnitude of the wake and located it higher in the pitchwise direction. All results gradually became slightly negative in value outside the wake, which may be caused by numerical inaccuracy as a result of the grid not being fine enough in these regions. The best results in terms of width of the wake region were obtained with the 8-million cell grid and RANS with k-epsilon turbulence and algebraic transition model. Results were poorer overall for the hybrid RANS/LES model as they greatly over- and underpredicted the wake for the 8-million and 32-million cell grids, respectively.

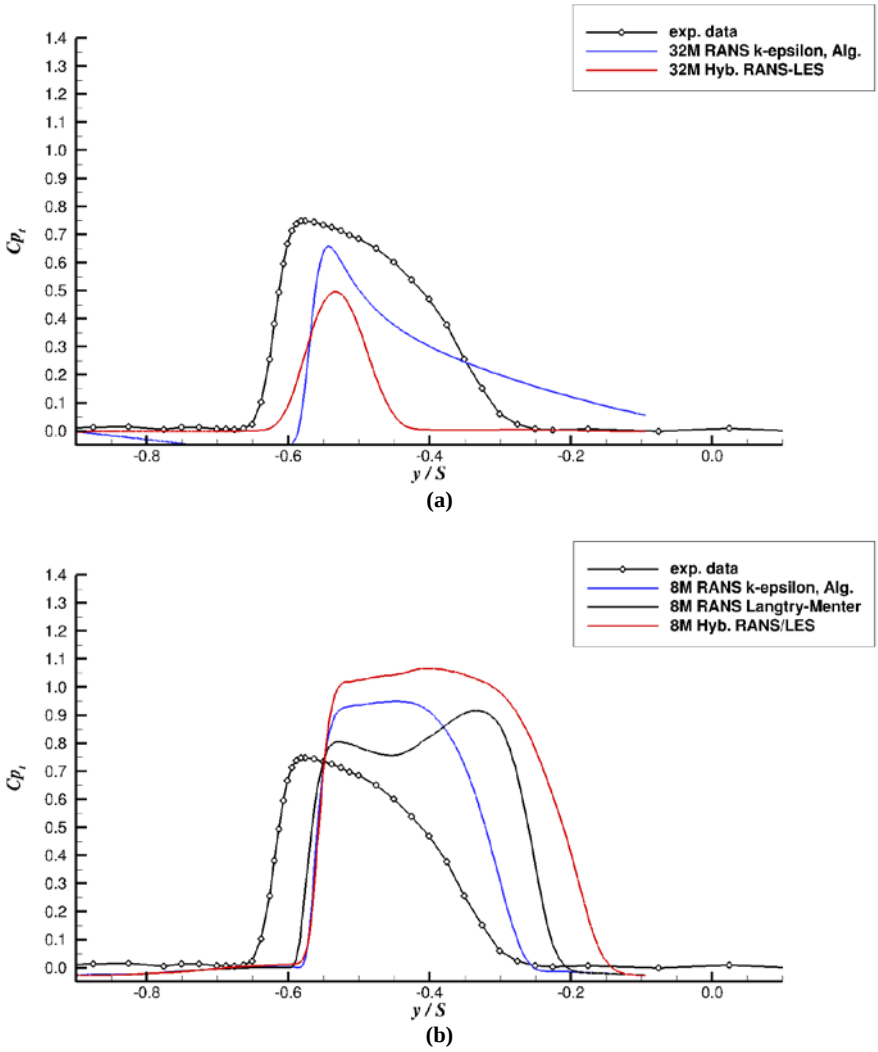

Fig. 5 Comparison of hybrid RANS/LES and RANS computations to experiment for cruise condition total pressure loss at 0.07 axial chord downstream of midspan location

4.1.3 Flow Visualization

Stream trace plots of the flow field at midspan were created to visualize the flow around the blade in the *x* and *y* directions. The stream traces were plotted along with entropy values to guide in locating regions of separation.

As can be seen from Figs. 6 and 7, for the 32-million-cell grid, with no endwall included, the hybrid RANS/LES model showed a shallow separation on the suction side near the trailing edge at approximately the 95% C_x location. The RANS with k-epsilon turbulence and algebraic transition model showed no separation on the suction side. No separation appeared on the pressure side for either model.

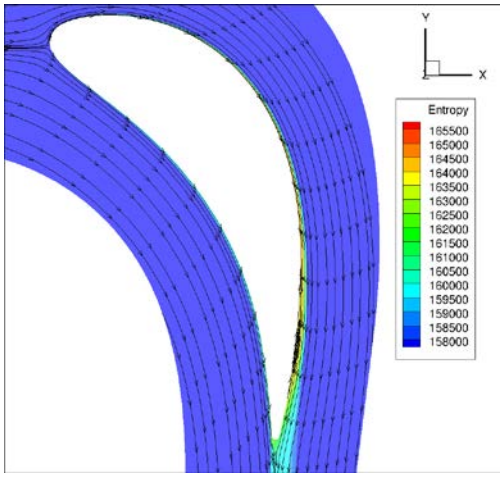

Fig. 6 Stream traces of hybrid RANS/LES solution and 32-million-cell grid for cruise condition

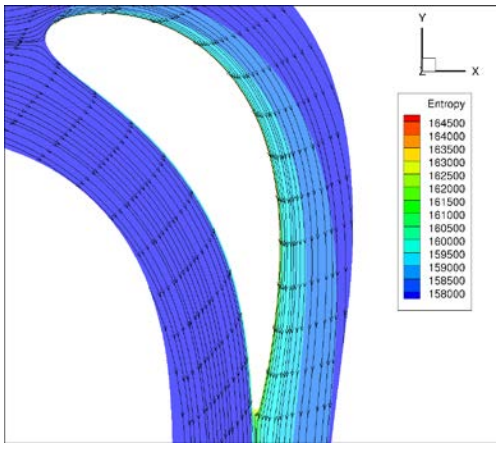

Fig. 7 Stream traces of RANS k-epsilon/Algebraic solution and 32-million-cell grid for cruise condition

In Figs. 8–10, the plots of both hybrid RANS/LES and RANS solutions using the 8-million-cell grid, with endwall included, show separations on the suction side after approximately 60% C_x. Both RANS models show a small separation bubble at approximately the 70% C_x location and another larger one close to the trailing edge at approximately the 90% C_x location. The hybrid RANS/LES model shows a vortex formation at approximately the 90% chord location. The hybrid RANS/LES model shows the largest vortex formation at this location followed by the RANS models, with the RANS with Langtrey-Menter turbulence/transition model showing the smallest vortex formation. No separation appeared on the pressure side for any model.

Differences between the predictions from the 2 grids again suggest the side wall is having a significant effect on the flow at midspan.

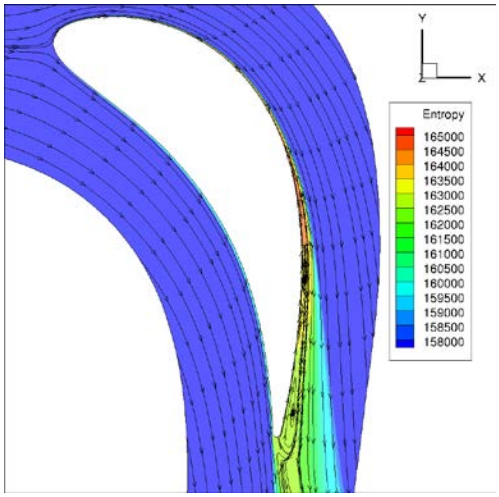

Fig. 8 Stream traces of RANS k-epsilon, Alg. solution and 8 million cell grid, endwall included, for cruise condition

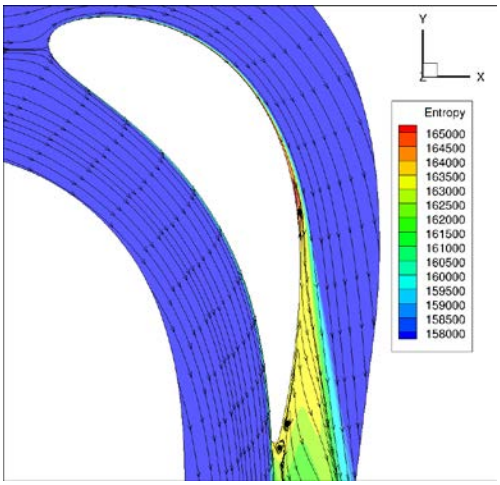

Fig. 9 Stream traces of RANS Langtry-Menter solution and 8-million-cell grid, endwall included, for cruise condition

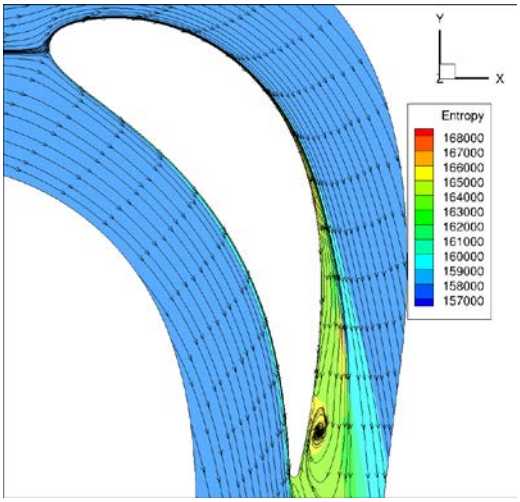

Fig. 10 Stream traces of hybrid RANS/LES solution and 8-million-cell grid for cruise condition

4.2 Takeoff Angle

4.2.1 Pressure Distribution

Comparisons of hybrid RANS/LES and time accurate RANS computational results to experimental measurements of the blade pressure distributions were made. Figure 11 compares solutions to experiment for blade surface pressures for the takeoff condition at the 50% span location. Figure 11a compares results using the 32-million-cell grid and Fig. 11b compares results using the 8-million-cell grid. Experimental results were measured on 3 consecutive blades in the cascade, blades 4–6, as shown in the legend. The highly negative incidence (–36.7°) produces an inverted pressure distribution in the leading edge region of the blade with the loading reverting to nominal beyond 20% of the chord from the leading edge.[12]

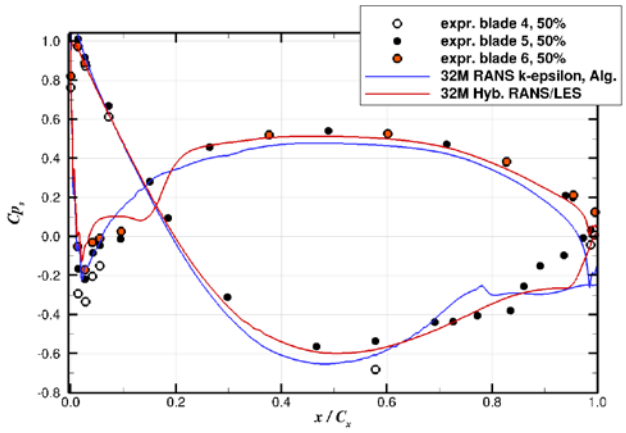

(a)

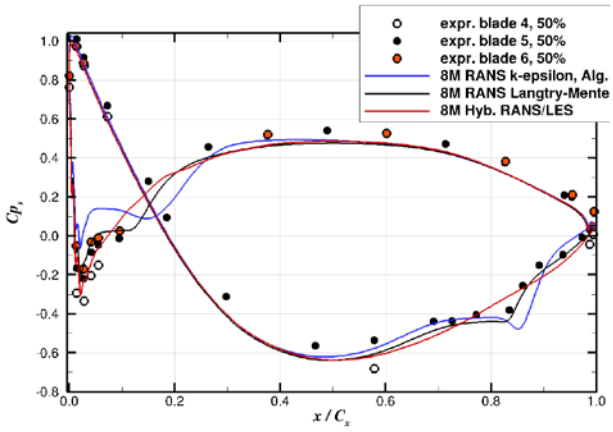

(b)

Fig. 11 Comparison of hybrid RANS/LES and RANS computations to experiment for takeoff condition pressure distributions at 50% span; a) 32M grid and b) 8M grid

As shown in Fig. 11a, the hybrid RANS/LES and the RANS model match the experimental data poorly on the suction side after x/C_x = 0.8 and do not correctly capture the plateau, suggesting possible separation at x/C_x = 0.7 – 0.85. On the pressure side, agreement between both models and the data is good; however, the RANS model failed to predict the plateau in the experimental data suggesting possible separation at x/C_x = 0.05 – 0.2. As shown in Fig. 11b, all 3 models compare well to experiment; however, the hybrid RANS/LES model failed to predict both plateaus in the experimental data on the suction and pressure sides. Both RANS models predict these plateaus with the Langtry-Menter model matching the data more closely. The k-epsilon turbulence and algebraic transition model predicted too wide a plateau for both regions and underpredicted the pressure drop on the pressure side and overpredicted the pressure drop on the suction side. Overall, the RANS simulation with Langtry-Menter model compared best for blade loadings. In the plots for both grids, the best comparisons are with the 8-million-cell grid, which further indicates this grid is a better predictive model of the experimental cascade blade.

4.2.2 Exit Total Pressure

Comparisons of computational results to experimental measurements for the blade wake region were made. Figure 12 compares plots of computed and measured midspan total pressure loss at 7% C_x downstream. The Hybrid RANS/LES model predicted the shape, size, and height of the wake with fair results, although there is some misalignment in the computed pitchwise location of the wake compared to measurements (Fig. 12a). There is further misalignment in the computed pitchwise location for the RANS solution using this grid and the shape, width, and the maximum Cp_t value are greatly overpredicted. In addition, RANS computed values of Cp_t outside the wake become slightly negative in value below the pressure side of the blade, which is inconsistent with the data. As shown in Fig. 12b, all results with the 8-million cell grid overpredicted the magnitude of the wake and located it higher in the pitchwise direction. The RANS with k-epsilon turbulence and algebraic transition model greatly overpredicted the width of the wake while the hybrid RANS/LES model matched it closest. Overall, the hybrid RANS/LES model using the 32-million-cell grid compared closest to the experimental data in terms of shape, width, height, and location.

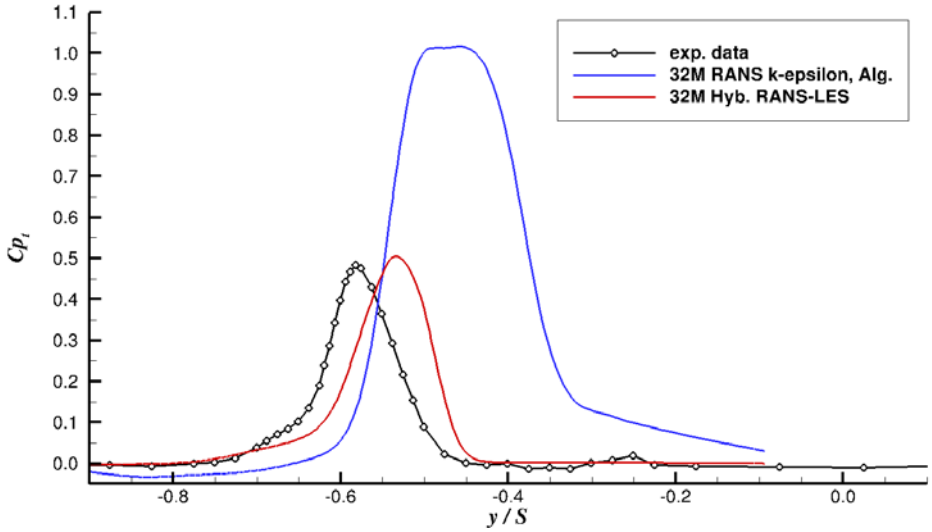

(a)

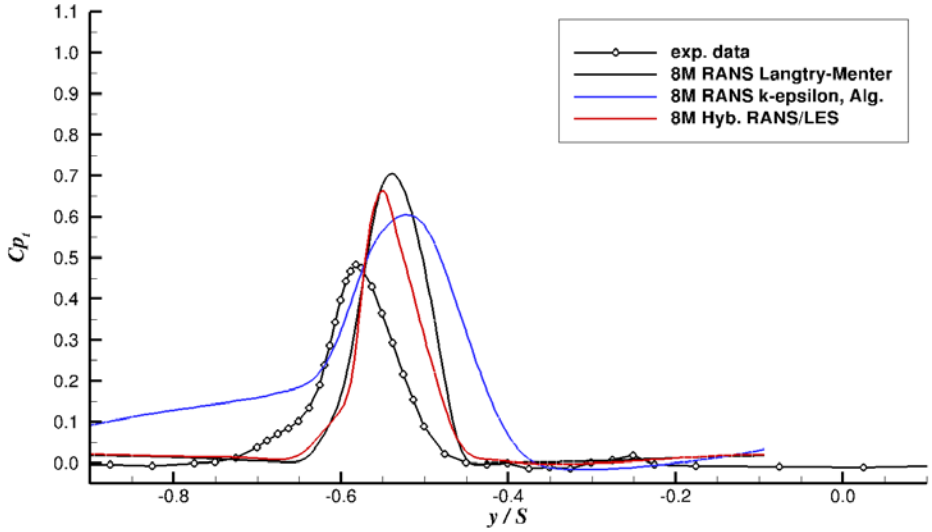

(b)

Fig. 12 Comparison of hybrid RANS/LES and RANS computations to experiment for takeoff condition total pressure loss at 0.07 axial chord downstream of midspan location

4.2.3 Flow Visualization

Stream trace plots of the flow field at midspan were created to visualize the flow around the blade in the *x* and *y* directions. The stream traces were plotted along with entropy values to guide in locating regions of separation.

In Fig. 13, the hybrid RANS/LES model with the 32-million-cell grid shows a shallow separation on the suction side closer to the trailing edge compared to the RANS solutions using the 8-million-cell grid. On the pressure side, the hybrid RANS/LES model predicted separation in the same area near the leading edge as the RANS solutions using the 8-million-cell grid. The size of the separation bubble appears similar to that of the RANS with k-epsilon turbulence and algebraic transition model using the 8-million-cell grid. In Fig. 14, the RANS with k-epsilon turbulence and algebraic transition model using the 32-million-cell grid showed the largest separation on the suction side starting at approximately $x/C_x = 0.75$ with no reattachment. No separation appeared on the pressure side for this model using this grid.

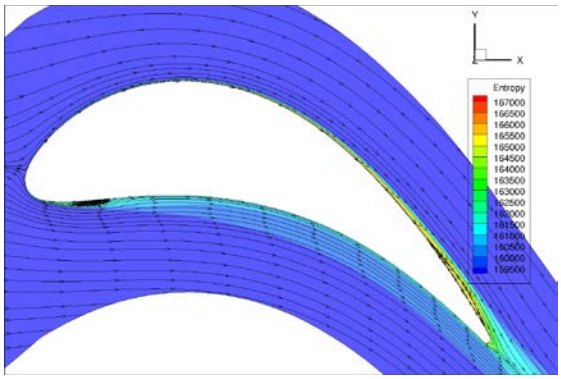

Fig. 13 Stream traces of hybrid RANS/LES solution and 32-million-cell grid for takeoff condition

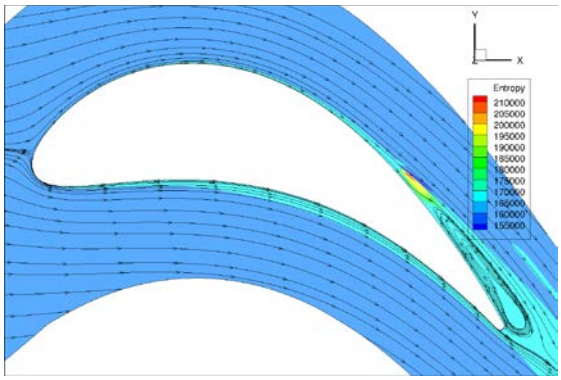

Fig. 14 Stream traces of RANS k-epsilon/Algebraic solution and 32-million-cell grid for takeoff condition

In Figs. 15 and 16, combined stream trace and entropy plots of both RANS solutions using the 8-million-cell grid, with endwall included, show shallow separation and reattachment near the trailing edge on the suction side at x/C_x = 0.7 – 0.9. On the pressure side, the plots of both RANS solutions show separation and reattachment close to the leading edge at approximately x/C_x = 0.05 – 0.15. The RANS solutions vary in predicting how large the separation bubbles are with the Langtry-Menter solutions predicting smaller sized ones. The hybrid RANS/LES model predicted no separation on either side of the blade using this grid (Fig. 17). Differences between the predictions from the 2 grids again reinforce the conclusion that the side wall has a significant effect on the flow at midspan.

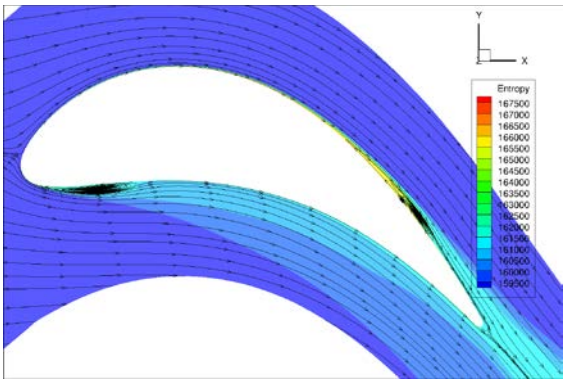

Fig. 15 Stream traces of RANS k-epsilon/Algebraic solution and 8-million cell grid, endwall included, for takeoff condition

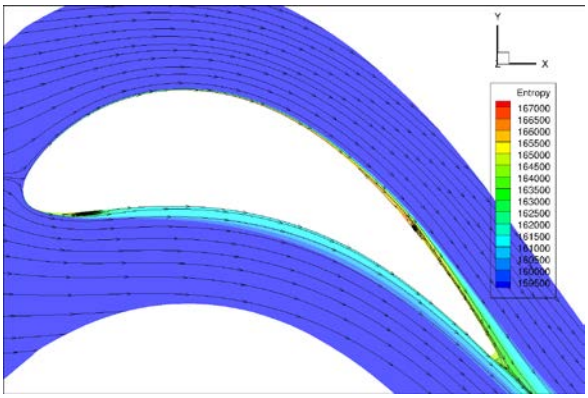

Fig. 16 Stream traces of RANS Langtry-Menter solution and 8-million cell grid, endwall included, for takeoff condition

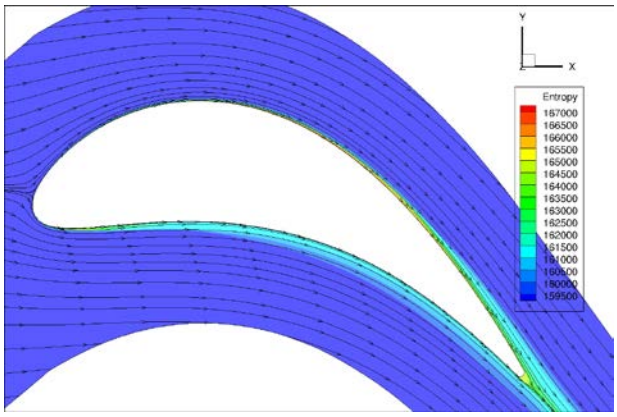

Fig. 17 Stream traces of hybrid RANS/LES solution and 8-million cell grid, endwall included, for takeoff condition

5. Conclusions

A study was performed comparing hybrid RANS/LES and unsteady RANS computations to better understand and predict unsteady separated flow of a linear VSPT cascade blade operating with large incidence angle variation. The computations comprised a periodic single blade that represents the midspan section of a VSPT blade that was tested in the NASA GRC Transonic Turbine Blade Cascade Facility. Simulations were assessed at low inlet turbulence levels for positive and negative incidence angles that represent turbine cruise and takeoff conditions. Two grids, a very refined one that included the center of the span and a fine grid that included the endwall, were used for the comparisons. Comparisons of results for blade loading and loss were made to experimental data from the transonic tunnel. Comparisons of results for separation predictions were made between the hybrid RANS/LES and RANS computations.

For pressure distributions, the RANS simulations with the Langtry-Menter model compared best to the experiments. For midspan total pressure loss, overall, no model compared well to the experiments. Errors in predicting the wake for the RANS simulations with the k-epsilon turbulence and algebraic transition model appear independent of Reynolds number as they were similar to those observed by Booth et al. 2015[14] at higher Reynolds number flow conditions using the same 8-million-cell grid and modelling technique. It was found that endwall effects have a significant influence on the flow at midspan for both flow conditions and the endwall should be included in the grid for future hybrid RANS/LES studies.

Separation prediction comparisons revealed significant differences in the presence of and extent of separation between the models and grid types. For the cruise condition the majority of simulations predicted shallow separations on the suction

side after approximately 60% C_x. For the takeoff condition, the majority of simulations predicted a shallow separation after approximately 70% x/C_x on the suction side and a shallow separation bubble close to the leading edge on the pressure side. Differences among the separation predictions were in bubble size, location, and whether the separation reattached. As there is no experimental data at this time to compare simulation results with respect to these characteristic attributes, the accuracy of the predictions may not be conclusive.

It was inconclusive as to how the hybrid RANS/LES model would perform compared to the RANS models. The shallowness of the predicted separations present challenges for hybrid RANS/LES simulations due to their presence within the anisotropic RANS mesh region of the grid, which can cause the simulation to predict the separation zones with the RANS instead of the LES algorithms of the model. Further investigation with a more refined grid in the boundary layer region should be performed to verify that the model uses LES simulation of the separation zones.

Further assessment is being done to determine if the higher fidelity of the hybrid RANS/LES model compared to RANS simulations performs more accurately to resolve the flow features necessary for accurate prediction of separation. Future work will include comparison studies of computational results to experiments when experimental separation and transition measurements become available. Comparisons at other Reynolds numbers and fluid stream turbulence levels will be made to understand sensitivity of results to changes in these conditions. In addition, comparing the accuracy of results of a periodic single blade grid to a grid that includes the full blade cascade passages may also be performed.

6. References

1. Spalart PR, Deck S, Shur ML, Squires KD, Strelets M Kh, Travin A. A new version of detached-eddy simulation, resistant to ambiguous grid densities. J Theor Comput Fluid Dyn. 2006;20(3):181–195.

2. Basu D, Hamed A, Das K. DES and hybrid RANS/LES models for unsteady separated turbulent flow predictions. AIAA-2005-0503. Proceedings of the 43rd AIAA Aerospace Sciences Meeting & Exhibit; 2005 Jan 10–13; Reno (NV).

3. D'Angelo M. Wide speed range turboshaft study. 1995 Aug. Report No.: NASA/CR–198380.

4. Welch GE. Assessment of aerodynamic challenges of a variable-speed power turbine for large civil tilt-rotor application. Proceedings of the 66th American Helicopter Society International Annual Forum, Phoenix (AZ); 2010 May 11–13; Fairfax (VA); American Helicopter Society International; c2010. p. 345; also NASA TM-2010-216758, 2010 Aug.

5. Flegel-McVetta AB, Giel PW, Welch GE. Aerodynamic measurements of a variable-speed power-turbine blade section in a transonic turbine cascade at low inlet turbulence. 2013 Aug. Report No.: NASA/TM–2013-218069.

6. Flegel AB, Giel PW, Welch GE. Aerodynamic effects of high turbulence intensity on a variable-speed power-turbine blade with large incidence and Reynolds number variations. AIAA-2014-3933. Proceedings of the 50th AIAA/ASME/SAE/ASEE Joint Propulsion Conference; 2014 July 28–30; Cleveland (OH). Reston (VA): American Institute of Aeronautics and Astronautics; c2014. p. 6166.

7. Welch GE, McVetta AB, Stevens MA, Giel PW, Ameri AA, To W, Skoch GJ, Thurman DR. Variable-speed power-turbine research at Glenn Research Center. Proceedings of the 68th American Helicopter Society International Annual Forum; 2012 May 1–3; Fort Worth (TX). Fairfax (VA): American Helicopter Society International; c2012. p. 2436; also NASA TM-2012-217605, 2012 July.

8. Xiao X, McCarter AA, Lakshminarayana B, Pugh E. Tip clearance effects in a turbine rotor: Part I—pressure field and loss. ASME J Turbomach. 2000;123(2):296–304.

9. Menter FR, Langtry R, Völker S. Transition modelling for general purpose CFD Codes. J Flow Turbulence Combust. 2006;77:277–303.

10. Verhoff VG, Camperchioli WP, Lopez I. Transonic turbine blade cascade testing facility. AIAA-92-4034. Proceedings of the 17th Aerospace Ground Testing Conference; 1992 July 6–8; Nashville (TN). Reston (VA): American Institute of Aeronautics and Astronautics; c1992.

11. Giel PW, Sirbaugh JR, Lopez I, Van Fossen GJ. Three dimensional Navier-stokes analysis and redesign of an imbedded bellmouth nozzle in a turbine cascade inlet section. ASME Journal of Turbomachinery. 1996;118(3):529–535; also NASA TM-107284, 1996 Oct; and US Army ARL-MR-152, 1996 July.

12. McVetta AB, Giel PW, Welch GE. Aerodynamic investigation of incidence angle effects in a large scale transonic turbine cascade. AIAA-2012-3879. Proceedings of the 48th AIAA/ASME/SAE/ASEE Joint Propulsion Conference & Exhibit; 2012 July 30–Aug 1; Atlanta (GA). Reston (VA): American Institute of Aeronautics and Astronautics; c2012. p. 1765.

13. Ford A, Bloxham M, Turner E, Clemens E, Gegg S. Design optimization of incidence-tolerant blading relevant to large civil tilt-rotor power turbine applications. 2012 Dec. Report No.: NASA/CR–2012-217016.

14. Booth DT, Flegel AB. Comparison of computational and experimental results for a transonic variable-speed power-turbine blade operating with low inlet turbulence levels. AIAA-2015-3928. Proceedings of the 51th AIAA/ASME/SAE/ASEE Joint Propulsion Conference; 2015 July 27–29; Orlando (FL). Reston (VA): American Institute of Aeronautics and Astronautics; c2015. p. 2593.

15. CFD++. Ver. 16.1.1 Agoura Hills (CA): Metacomp Technologies, Inc. 2015. [accessed 2017 Sep 5].

16. CFD++ and CAA++ User manual, Ver. 11.1. Agoura Hills, (CA). Metacomp Technologies, Inc. 2015 [accessed 2017 Sep 5].

17. Shur ML, Spalart PR, Strelets M, Kh, Travin AK. A hybrid RANS-LES approach with delayed-DES and wall-modelled LES capabilities. Int J Heat Fluid Flow. 2008;29(6):1638–1649.

18. Batten P, Goldberg U, Kang E, Chakravarthy S. Smart sub-grid-scale models for LES and hybrid RANS/LES. AIAA-2011-3472. Proceedings of the 6th AIAA Theoretical Fluid Mechanics Conference; 2011 June 27–30; Honolulu

(HI). Reston (VA): American Institute of Aeronautics and Astronautics; c2011. p 674.

19. Batten P, Goldberg U, Chakravarthy S. Interfacing statistical turbulence closures with large-eddy simulation. AIAA Journal. 2004;42(3):485–491.

20. Pointwise. Ver. 17.3. Fort Worth, (TX): Pointwise, Inc. 2015. [accessed 2017 Sep 5]. http://www.pointwise.com/news/Pointwise-V173R2-Released.shtml.

21. White FM. Viscous fluid flow. 3rd ed. New York (NY): McGraw Hill; 2006. Chap. 6.

22. Ameri A. Requirements for large eddy simulation computations of variable-speed power turbine flows. 2016 Apr. Report No.: NASA/CR–2016-218962.

23. Thurman DR, Flegel AB, Giel PW. Inlet turbulence and length scale measurements in a large-scale transonic turbine cascade. AIAA-2014-3934. Proceedings of the 50th AIAA/ASME/SAE/ASEE Joint Propulsion Conference; 2014 July 28–30; Cleveland (OH). Reston (VA): American Institute of Aeronautics and Astronautics; c2014. p 6184.

List of Symbols, Abbreviations, and Acronyms

2-D	2-dimensional
3-D	3-dimensional
ARL	US Army Research Laboratory
CFD	Computational Fluid Dynamics
COTS	commercial off-the-shelf
Cp_s	static pressure coefficient, $Cp_s = (P - P_2)/(P_{t,1} - P_2)$
Cp_t	total pressure coefficient, $Cp_t = (P_{t,1} - P_t)/(P_{t,1} - P_2)$
C_x	blade axial chord
GRC	NASA Glenn Research Center
H	blade span
i	incidence angle (degree), $i = \beta_1$ – inlet metal angle (34.2^o)
M	Mach number
NASA	National Aeronautics and Space Administration
P	static pressure
PR	pressure ratio, $PR = P_1/P_2$
P_t	total pressure
RANS/LES	Reynolds-averaged Navier-Stokes/Large-Eddy Simulation
RHS	right-hand side
Re	Reynolds number, $Re = \rho U C_x/\mu$
S	blade pitch
SGS	sub-grid scale
Tu	turbulence intensity, $Tu = SQRT(ave\ u'^2_s + ave\ u'^2_z)/U$
u'	fluctuating component of velocity
U	free stream velocity

VSPT	variable-speed power-turbine
Δy_{init}	initial distance from the wall to the first wall-adjacent centroid
x	axial coordinate
y	pitchwise coordinate
z	spanwise coordinate
δ	boundary layer thickness
μ	dynamic viscosity
ρ	density
β_1	relative inlet flow angle (degree), $\beta_1 = \tan^{-1}(U_y / U_x)$

Subscripts

1	based on inlet condition
2	based on exit condition
b	baseline
is	isentropic value
s	streamwise component
t	total condition

1 DEFENSE TECHNICAL
(PDF) INFORMATION CTR
DTIC OCA

2 DIR ARL
(PDF) RDRL DCM
IMAL HRA RECORDS MGMT
RDRL DCL
TECH LIB

1 GOVT PRINTG OFC
(PDF) A MALHOTRA

1 DIR USARL
(PDF) RDRL VTP
D BOOTH